PHYSICAL REVIEW C VOLUME 19, NUMBER 3 MARCH 1979

Absolute cross sections for three-body breakup reactions ^{6}Li(d, n ^{3}He)^{4}He and ^{6}Li(d, p ^{3}H)^{4}He

R. E. Holland, A. J. Elwyn, C. N. Davids, F. J. Lynch, L. Meyer-Schützmeister, J. E. Monahan, F. P. Mooring, and W. Ray, Jr.
Argonne National Laboratory, Argonne, Illinois 60439
(Received 6 September 1978)

Absolute cross sections have been obtained for the reactions ^{6}Li(d,n ^{3}He)^{4}He and ^{6}Li(d,p ^{3}H)^{4}He for deuteron energies from 100 to 800 keV. The energy spectra of particles from these reactions are continuums because of the three-body final state. Total cross sections as well as angular distributions have been obtained with accuracies of 10 to 17%. Comparisons of energy spectra are made to predictions of simple models.

[NUCLEAR REACTIONS ^{6}Li(d,p^3H)^{4}He, E_d = 0.1–0.8 MeV, ^{6}Li(d, n^3He)^{4}He, E_d = 0.2–0.8 MeV; enriched target; measured $\sigma(E_d, \theta, E_n)$, $\sigma(E_d, \theta, E_p)$, $\sigma_t(E_d)$.]

I. INTRODUCTION

This paper is one of a series[1-3] in which we examine experimentally the various reactions induced by deuterons incident on ^{6}Li at energies between 100 and 1000 keV. In the present paper we present measurements of the reactions ^{6}Li(d,n^3He)^{4}He and ^{6}Li(d,p^3H)^{4}He which result in three-body final states. Our objective in these measurements was to obtain reliable total cross sections for reactions which are relevant to the design of "advanced" fusion reactors[4] and to calculations of certain astrophysical processes.[5]

Because of the three-body final state for these reactions, the energy spectra are continuums, and very little work has been done in measuring these cross sections. In addition to investigations[6] at much higher energies, various groups[7] have studied the particle spectra at bombarding energies near 1 MeV, but without obtaining cross sections. Macklin and Banta[8] measured the cross section for tritium production from ^{6}Li(d,p^3H)^{4}He from 400 keV to 4 MeV. This latter measurement should, of course, yield exactly the same values as our measurement of the cross section for continuum proton production when the proton spectra are integrated over energy and angle. These two measurements, taken in different laboratories by quite different techniques, are in excellent agreement.

Figure 1 presents a portion of the mass-8 nuclear energy-level diagram[9] which is relevant for this investigation. In the absence of an interaction between the final particles, it is expected that the energy spectra of the particles will be directly proportional to the phase space[10] available to them. However, the reaction leading to the final state, consisting of $n + ^3$He $+ ^4$He, should be visualized not only as a direct breakup into three particles, but also as partly proceeding through the ground state of ^{5}He which then decays into a neutron and ^{4}He. States in ^{7}Be which also might serve as intermediate states in this sequential decay model are not shown in Fig. 1, since there are none in the energy region applicable to this work. Similarly, for breakup into $p + ^3$H $+ ^4$He $+ ^4$He, sequential decays can occur through the ground state of ^{5}Li and the second excited state of ^{7}Li at 4.63 MeV. These discrete states in the sequential decay model represent final-state interactions which modify the phase-space energy distributions otherwise expected. When the intermediate states of the unobserved pair are relatively well defined in energy (and therefore relatively long lived), one can then expect a peak superimposed on the phase-space energy spectrum. This is the situation for transitions through the state in ^{7}Li at 4.63-MeV excitation where the effect of the state is to produce a well-defined peak in the proton continuum. For the broader, less-well-defined states as in ^{5}He and ^{5}Li, the effects are more difficult to identify in spectra in which only one final-state particle is observed. A broad peak appears in the mass-3 energy spectrum at a position that could include the expected peaks from the ground states of ^{5}Li and ^{5}He. In addition, we expect that at the relatively low energies involved here, the Coulomb interaction will strongly modify the phase-space spectrum. A prescription[11] which treats the Coulomb interaction in the sequential decay model was used to calculate the effects on the spectrum near the upper energy limit. This method takes into account the Coulomb interaction between the two unobserved particles, but ignores their interaction with the detected particle. One expects this treatment of the Coulomb interaction to be more nearly

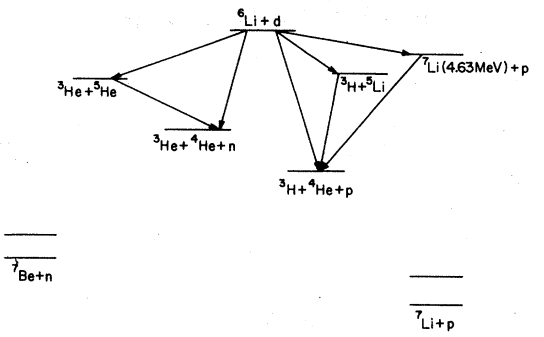

FIG. 1. A partial energy level diagram for $A=8$. Only levels of interest for three-body final states are shown.

correct when the energy of the observed particle is large and when the observed particle is a neutron.

As the discussion above implies, we have in the present work studied only the single-particle spectra in these reactions rather than kinematically complete coincidence spectra. In addition, because of the three-body final states, center-of-mass spectra are not easily obtained from the observed spectra. (Different energy increments of the observed spectrum at a given laboratory angle correspond to different center-of-mass angles; so in order to obtain center-of-mass continuum spectra, measurements have to be made at a large number of closely spaced laboratory angles). Thus we have preferred to give our results in the laboratory system and, where comparisons are made to results derived in the center-of-mass system, to make the comparison in the laboratory system.

In addition to the measurement of total cross sections, which was our primary objective, we were able to observe effects of final-state interactions. Also, because spectra were obtained for each of the particles emitted in the reactions ^{6}Li$(d,p^3$H$)^4$He and ^{6}Li$(d,n^3$He$)^4$He, we were able to use a number of relationships between the total cross sections for these particles, including that mentioned above for tritium production, in order to test the accuracy of our results. This procedure is particularly satisfying when the neutron data are considered, since the experimental techniques are then quite different.

The remainder of this paper contains a discussion of the techniques of measurement, the results of the measurement, the accuracy and reliability of the results and a comparison to the predictions of some simple models.

II. EXPERIMENT

The measurements of the neutron continuum spectra were obtained simultaneously with measurements of the ^{6}Li$(d,n)^7$Be reactions to the ground and first excited state of ^{7}Be. The techniques for these time-of-flight neutron measurements have been discussed earlier[1]; we shall review them briefly here.

The experiments were performed at the Argonne 4-MV Dynamitron accelerator. The $^2H_3^+$ molecular deuterium beam was used because this made it possible to obtain low-energy deuterons while running the accelerator with a higher terminal voltage where the operation is more stable. Targets were made of LiF (enriched to 99.3% in ^{6}Li) evaporated on thick tantalum backings, which formed both a vacuum wall and also the end of the Faraday cup (which collected the beam current). These targets of LiF were very stable, much more so than metallic Li, and although reactions of the deuterons with ^{19}F could be observed at the higher energies, the cross sections were low and the contaminant peaks could be easily subtracted from the spectra. The thickness of these targets was obtained by measuring the energy loss of back-scattered deuterons as described earlier.[1] The results of these energy-loss measurements were found to agree to within 5% with measurements of target thickness obtained from Rutherford scattering. The current integrator was calibrated several times throughout the experiment with a battery of known voltage and precision resistors, and was always found within 0.5% of its nominal calibration. Charge-collection efficiency was also checked to verify that it was within a few percent of unity.

The measurements of neutron cross sections were made with a deuteron beam pulsed with a repetition rate of 1 MHz and with a pulse width of 1.2 ns. Neutrons were detected in stilbene scintillators (with a threshold for neutron detection of about 400 keV) at distances between 2 and 3.8 m from the target. Detector efficiencies were obtained by measuring ^{7}Li$(p,n)^7$Be neutrons from targets of known thickness, from ^{2}H$(d,n)^3$He neutrons detected in coincidence with ^{3}He particles and by calculations[1,12] from known geometry and scintillator response. Measured counts per channel were corrected for background and efficiency and converted into differential cross sections per unit energy interval. These distributions were extrapolated linearly to zero energy from the neutron detector threshold and then integrated to the maximum neutron energy at which breakup can occur for each deuteron energy in order to obtain differential cross sections at each angle. A complete description of the electronic equipment for the neutron time-of-flight measurements has been given[12] and details relative to the present measurements of neutron continuum spectra appear in earlier publications,[1,2] which describe work done

simultaneously with the ^{6}Li$(d,n)^7$Be measurements.

The target chamber for the charged-particle measurements was the same chamber (76 cm diameter) as that used for the ^{6}Li$(d,p)^7$Li measurements.[3] Again the $^2H_3^+$ molecular beam from the Argonne 4-MV Dynamitron was used to allow us to reach low bombarding energies with reasonable terminal voltages in the accelerator. The ion beam entered the chamber through two defining apertures 1.5 mm in diameter and 25 cm apart, passed through a thin target in the center of the chamber, and stopped in a Faraday cup beyond the chamber. The targets consisted of 75–100 μg/cm^2 of LiF enriched to 99.3% in ^{6}Li evaporated onto thin (10–15 μg/cm^2) carbon films. Yields of charged particles were obtained relative to the yield of protons from the ^{6}Li$(d,p)^7$Li reaction, the cross sections for which we had measured earlier.[3] Thus the derived continuum cross sections do not depend on measurement of the ion-beam current, nor critically on the target thickness (except insofar as the target thickness influenced the mean incident deuteron energy).

Because the spectra of protons, ^{3}H, ^{3}He, and ^{4}He (as well as the spectra of recoiling higher masses) were overlapping continuums, the deuteron beam was pulsed to allow the mass of the detected particle to be identified by time of flight; the energy was determined from the pulse height in the Si surface-barrier detector since the short flight path available did not allow good energy resolution by time of flight. The beam pulse rate in this case was 8 MHz with a pulse width of about 1 ns, and the flight path from target to detector was 25 cm. Time and pulse-height data were stored as a two-dimensional array, 256 × 256 channels, in a PDP 11/45 computer. A simple transformation from an energy-vs-time array to an energy-vs-mass array allowed us to produce energy spectra for each of the low masses in the following manner.

For each set of data, a mass-vs-energy array was obtained from the time-vs-energy array by applying to each element labeled by (T,E) the transformation

$$M = K(T - T_0)^2 E ,$$

and adding to the location (M,E) in the new array, the contents of the location (T,E). The constant K (which depends on the distance between target and detector) and the constant T_0 (which is the time channel corresponding to zero time) could, in principle, be determined from separate measurements on the system. We preferred to infer them directly from the data. The value of K merely determined the mass scale and was chosen to produce a convenient range of masses. The other constant T_0 could be estimated by inspection of the data and then adjusted to produce the mass peaks at the same channels, independent of energy. There was no difficulty in interpreting the mass spectrum because each mass has a characteristic energy spectrum.

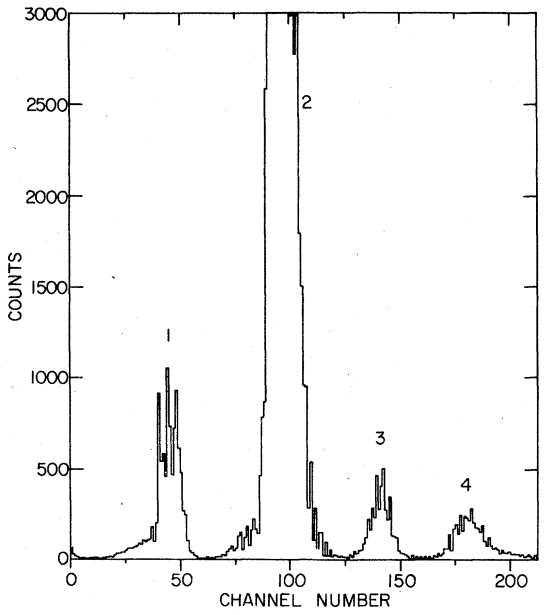

FIG. 2. Spectrum of masses observed for deuterons on ^{6}Li at a laboratory angle of 65° for a deuteron energy of 578 keV.

The mass resolution can be estimated from Fig. 2; it shows the mass spectra obtained after summing over particle energy. The mass-3 peak contains both ^{3}H and ^{3}He, and the mass-4 peak, while it is all ^{4}He, contains contributions from

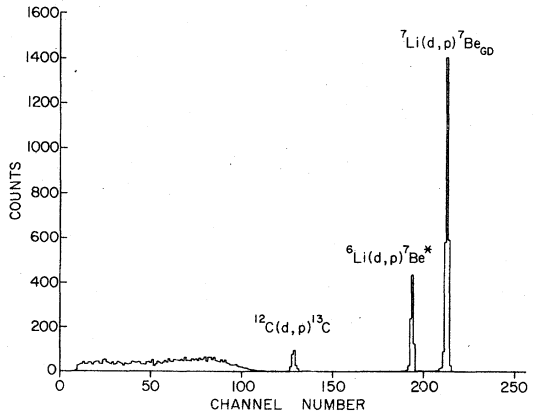

FIG. 3. Pulse height spectrum of protons from ^{6}Li + d reactions at a deuteron energy of 371 keV and laboratory angle of 90°

TABLE I. Differential cross sections (in the laboratory system) for continuum neutrons (summed over energy) from ^{6}Li$(d,n^3$H$)^4$He.

$\bar{E}_d$ (MeV)	$\sigma(\theta_{lab})$ (mb/sr) 0°	30°	60°	75°	111.6°	126.5°	148.5°
0.204	0.61	0.65	0.69	0.56	0.55	0.57	0.54
0.238	0.79	1.07	0.75	0.71	0.79	0.74	0.96
0.375	2.78	2.62	2.56	2.32	1.97	2.00	1.76
0.578	6.28	5.28	4.58	4.21	3.33	3.16	2.90
0.779	11.16	8.60	6.48	6.42	4.91		3.71

TABLE II. Differential cross sections (in the laboratory system) for continuum protons (summed over energy) from ^{6}Li$(d,p^3$H$)^4$He.

$\bar{E}_d$ (MeV)	$\sigma(\theta_{lab})$ (mb/sr) 25°	35°	45°	65°	90°	105°	125°	135°	145°	157°
0.117			0.105		0.081			0.095		
0.184			0.625	0.482	0.464		0.633			0.601
0.269			2.547	2.036	1.80	1.96	1.89		1.99	1.90
0.371		5.823	5.94	4.20	3.62	3.86	3.73		3.70	3.75
0.575	16.67		11.69	9.058	8.098	8.26	7.69		7.744	7.571
0.772	20.24		14.09	10.67	10.55	9.97	9.826		9.068	9.418

TABLE III. The coefficients (in the laboratory system) for the expansion, in a series of Legendre polynomials, of the differential cross section of continuum neutrons (summed over energy) for ^{6}Li$(d,n^3$He$)^4$He. The indicated errors are those obtained from the least-squares fitting procedure and do not include systematic errors.

$\bar{E}_d$ (MeV)	B_0	B_1	B_2 (mb/sr)	B_3	B_4
0.204	0.586 ± 0.018	0.052 ± 0.026			
0.238	0.779 ± 0.040	−0.028 ± 0.070	0.119 ± 0.086		
0.375	2.217 ± 0.030	0.516 ± 0.042	0.020 ± 0.058		
0.578	3.984 ± 0.073	1.485 ± 0.115	0.439 ± 0.161		
0.779	5.883 ± 0.029	2.628 ± 0.046	0.455 ± 0.065	0.500 ± 0.081	0.669 ± 0.124

TABLE IV. The coefficients (in the laboratory system) for the expansion, in a series of Legendre polynomials, of the differential cross section of the continuum protons (summed over energy) from ^{6}Li$(d,p^3$H$)^4$He. The indicated errors are those obtained from the least-squares fitting procedure and do not include systematic errors.

$\bar{E}_d$ (MeV)	B_0	B_1	B_2 (mb/sr)	B_3	B_4
0.117	0.083 ± 0.009	0.022 ± 0.014			
0.184	0.552 ± 0.040	−0.039 ± 0.068			
0.269	2.11 ± 0.045	0.49 ± 0.10	0.57 ± 0.12	0.34 ± 0.12	
0.371	4.33 ± 0.09	1.39 ± 0.19	1.38 ± 0.24	0.79 ± 0.24	
0.575	9.38 ± 0.10	3.53 ± 0.19	3.19 ± 0.26	2.27 ± 0.29	1.05 ± 0.28
0.772	11.5 ± 0.13	4.22 ± 0.24	3.80 ± 0.33	3.17 ± 0.38	1.84 ± 0.40

TABLE V. Total cross sections for the neutrons, protons, mass-3 particles, and mass-4 particles from ^{6}Li$(d,p^3$H$)^4$He and ^{6}Li$(d,n^3$He$)^4$He. The indicated errors include statistical errors and estimates for all systematic errors.

$\bar{E}_d$ (MeV)	σ_t(protons) (mb)	σ_t(mass-3) (mb)	σ_t(mass-4) (mb)	$\bar{E}_d$ (MeV)	σ_t(neutron) (mb)
0.117	1.04 ± 0.18	1.75 ± 0.25	1.67 ± 0.22		
0.184	6.94 ± 0.86	9.25 ± 1.28	9.04 ± 1.21	0.204	7.36 ± 1.10
0.269	26.5 ± 2.5	39.3 ± 4.1	38.0 ± 4.6	0.238	9.79 ± 1.60
0.371	54.4 ± 5.1	81.8 ± 8.8	79.4 ± 9.8	0.375	27.9 ± 4.2
0.575	118 ± 11	191.0 ± 19.2	180.0 ± 18.1	0.578	50.1 ± 7.5
0.772	145 ± 13	243.8 ± 22.9	224.9 ± 22.4	0.779	73.9 ± 10.4

both reactions ^{6}Li$(d,n^3$He$)^4$He and ^{6}Li$(d,p^3$H$)^4$He, which have differing endpoint energies. The quantized nature of the initial data (256 by 256 channels) produces a granular effect in the transformed mass distribution. This is evident in Fig. 2, but it has no effect on the energy distributions and is of no importance for the cross-section data. Figure 3 gives a typical pulse-height spectrum observed in the Si detector for protons.

In these data on the continuum charged particles the lower limit on the energy that could be detected was in the region of 200 to 600 keV. However, the energy distribution of the continuum particles extends to zero energy. Since the phase-space distribution approaches zero at zero energy, we used a linear extrapolation to obtain the yields at lower energies. The associated error was assumed to be due largely to uncertainties in the true energy distribution at low energies. We rather arbitrarily took the error to be one third of the correction in the extrapolation to zero energy. After this extrapolation, the continuum yield for each particle at each angle was summed and the cross section as a function of angle obtained from

$$\sigma(\theta)=\left[\sum_E Y(\theta,E)\right]\sigma(\theta,p)/Y(\theta,p)\,,$$

where $\sum_E Y(\theta,E)$ is the yield of continuum particles at the laboratory angle θ, summed over their energy, E; $\sigma(\theta,p)$ is the cross section for proton transitions to the two well-defined states in ^{7}Li through the reaction ^{6}Li$(d,p)^7$Li; and $Y(\theta,p)$ is the yield of protons to the same states in the present data. We took $\sigma(\theta,p)$ from our earlier measurements.[3]

The laboratory differential cross sections $\sigma(\theta)$, which are given in Tables I and II for neutrons and protons, were expanded in a series of Legendre polynomials. The coefficients of this expansion are given in Tables III and IV for neutrons and protons. The errors given in Tables III and IV for the expansion coefficients are the errors from the fitting program and represent the statistical errors modified by the internal consistency of the data. The total cross sections, representing integrations over energy and angle of the differential cross sections, are given by $\sigma_t=4\pi B_0$, where B_0 is the coefficient of the zeroth order Legendre polynomial. A similar procedure was used to obtain the total cross sections for mass-3 and mass-4 nuclei which were used in constructing Figs. 6 and 7.

In addition to errors given in Tables I–IV, which are mainly statistical, there are also systematic errors which contribute to the total error. For the charged-particle spectra these come primarily from the process of extrapolating the energy spectra to zero energy and from systematic errors in the ^{6}Li$(d,p)^7$Li cross section such as errors in target thickness and charge integration. These must be added in quadrature to the errors given in Tables I–IV to get the total errors. The total cross sections, with the total error, are given in Table V for continuum neutrons and continuum charged particles from ^{6}Li$(d,n^3$He$)^4$He and ^{6}Li$(d,p^3$H$)^4$He.

III. RESULTS AND DISCUSSION

We wish in this section to discuss the observed energy spectra from ^{6}Li$(d,p^3$H$)^4$He and ^{6}Li$(d,n^3$He$)^4$He reactions. A useful starting point for a discussion of the continuum spectra from three-body final states is the phase-space energy distribution[10] of one observed particle in the center-of-mass for the reaction. For our case this energy distribution is

$$P(E)dE\propto[(E_{\max}-E)E]^{1/2}dE\,, \qquad (1)$$

where E is the particle energy and $E_{\max}$ is its kinematically allowed maximum value. Equation (1), after transformation to the laboratory system, is the appropriate half ellipse shown on the energy distributions in Figs. 4 and 5.

The Coulomb force can be expected to influence

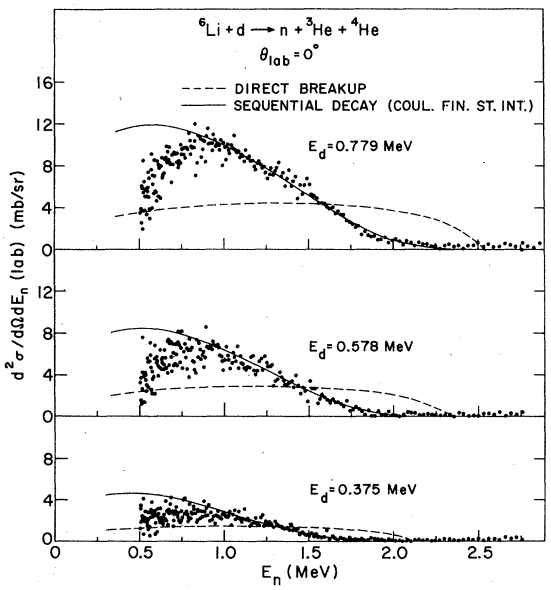

FIG. 4. Energy spectra of continuum neutrons from ^{6}Li$(d,n^3$He$)^4$He for several deuteron energies at a laboratory angle of 0°. The dashed curve is the phase-space distribution of Eq. (1); the solid curve is the Coulomb-corrected distribution calculated according to Eq. (2). Both calculated distributions have been transformed to the laboratory system.

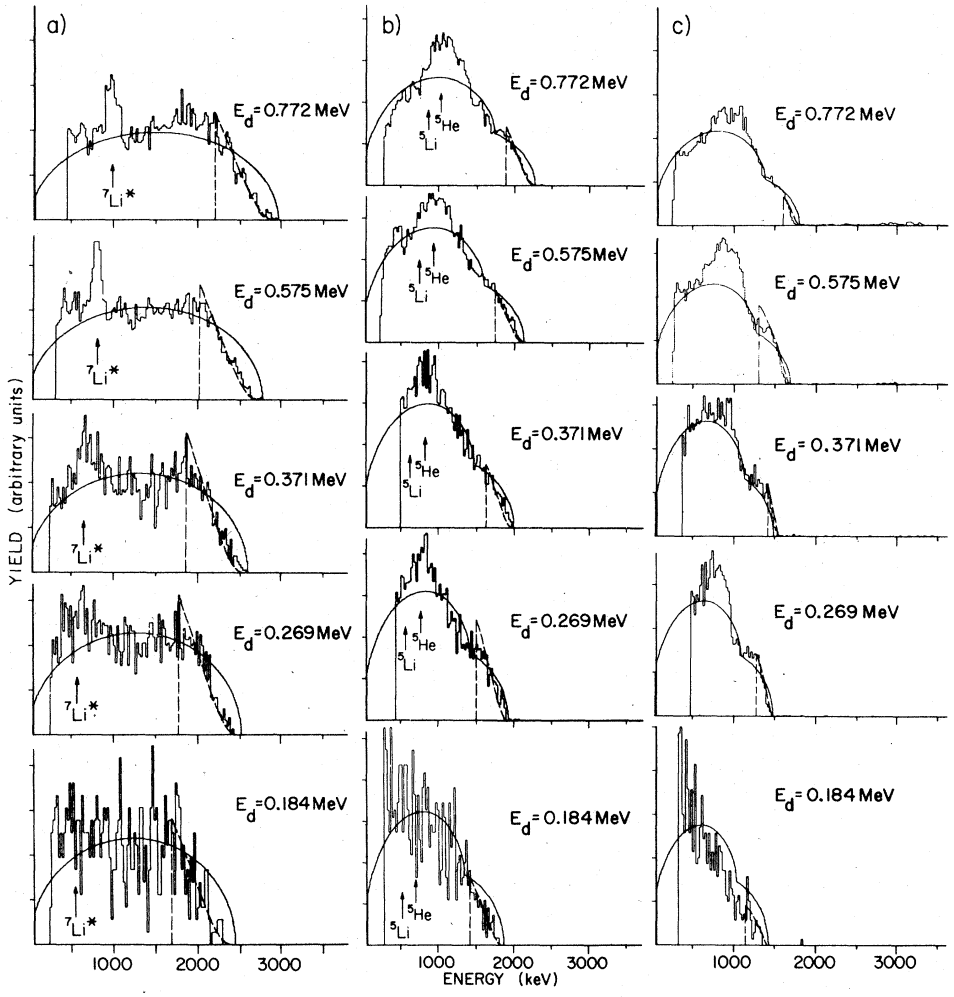

FIG. 5. (a) Energy spectra of the proton continuum at a laboratory angle of 65° and at a number of incident deuteron energies. The solid curve is the phase-space distribution of Eq. (1) after transformation to the laboratory system. The Coulomb-corrected energy distribution is shown as a dashed curve for the upper end of the spectrum. The peak arising from the ^{7}Li (4.63 MeV) state is indicated by an arrow. (b) Energy spectra of the continuum mass-3 particles at a laboratory angle of 65° and at a number of deuteron energies. The spectrum contains ^{3}H from ^{6}Li$(d,p^3\mathrm{H})^4$He and ^{3}He from ^{6}Li$(d,n^3\mathrm{He})^4$He. The phase space distribution is the solid curve which is the sum of two distributions calculated from Eq. (2), whose areas were determined as described in the text. The Coulomb corrected curve is shown as a dashed curve only for ^{3}H near the maximum allowed energy. The expected positons of peaks coming from transitions to ^{5}Li and ^{5}He are shown by arrows. (c) Energy spectra of ^{4}He particles from ^{6}Li$(d,n^3\mathrm{He})^4$He and ^{6}Li$(d,p^3\mathrm{H})^4$He at a laboratory angle of 65°. The phase-space distribution is the solid curve calculated by combining the contributions from the two reactions as described in the text. The Coulomb-corrected energy distribution is shown only near the maximum allowed energy as a dashed curve.

the energy distribution. One method for calculating the effect of the Coulomb interaction[11] makes use of the sequential decay model. When the Coulomb interaction with the observed particle is neglected and only the Coulomb interaction of the two unobserved particles is considered, the energy distribution of the observed particle in the center-of-mass system becomes

$$P(E)dE \propto C_0^2[(E_{\max}-E)E]^{1/2}dE\ , \qquad (2)$$

where

$$C_0^2 = 2\pi\eta/[\exp(2\pi\eta)-1]$$

and

$$\eta = Z_1 Z_2 e^2/\hbar u\ .$$

Here Z_1e and Z_2e are the charges of the unobserved particles and u is their relative velocity. This may be expected to be a particularly good approximation when the observed particle is a neutron

since its Coulomb interaction with the other particles is zero. Neutron spectra at zero degrees for several bombarding energies are shown in Fig. 4. Even for the neutron spectra, one can expect deviations between the Coulomb-modified phase-space distribution and the observed distributions. In the first place, the relative angular momentum of the unobserved pair is assumed zero; and second, other final-state interactions—for example, the interaction between the neutron and ^{4}He (to form ^{5}He)—have not been taken into account. The latter interaction can produce a peak in the energy distribution of tritons, but its effect on the neutron spectrum is spread by recoil effects so that it is very difficult to identify. For our data, the neutron spectra, at least in the higher energy region, are well described by the approximate Coulomb correction to the phase-space distribution as shown in Fig. 4.

Similar arguments can be used to interpret proton spectra from $^6\mathrm{Li}+d\rightarrow p+^3\mathrm{H}+^4\mathrm{He}$. In this case, however, one expects that the Coulomb modification described above will be less successful since there are additional Coulomb interactions between the proton and each of the unobserved particles which have not been included in the calculation. The results for protons are shown in Fig. 5(a). The calculation with the Coulomb correction according to Eq. (2) is shown as a curve covering approximately the upper 20% of the energy distribution. It was normalized to have the same area over the channels where it is shown as the measured energy distribution. At lower proton energies it differs widely from the observed spectrum. The phase-space energy distribution given by Eq. (1) and transformed to the laboratory system is shown as an approximate semiellipse. In Fig. 5(a) one also sees a nice illustration of a final-state interaction in the observed peak in the proton yield which arises from transitions to the 4.63-MeV state in ^{7}Li. This state is unstable to decay to $^3\mathrm{H}+^4\mathrm{He}$, with a width of ~100 keV, so that proton transitions to it produce a well-defined peak superimposed on the phase-space distribution. However, the particles (^{3}H and ^{4}He) from the breakup of this state do not produce any recognizable effect in the ^{3}H or ^{4}He spectrum because the ^{7}Li recoil velocity is added to their relative velocities in a manner which distributes the peak over a large region of their energy distributions.

Figure 5(b) displays similar spectra for the mass-3 particles (^{3}H and ^{3}He) from the reactions of $^6\mathrm{Li}+d$. In this case, two phase-space distributions were calculated (one for ^{3}H and one for ^{3}He) and added. The ratio of their areas in the center-of-mass system was simply the ratio predicted by the phase-space model described by Eq. (6) below. This composite curve was adjusted to have the same area as the measured data including the extrapolation to zero energy. The results in Fig. 5(b) are typical comparisons. Also shown in Fig. 5(b) is a calculation in which the phase-space distribution is modified by the Coulomb interaction as discussed above. Again, as with the proton spectra, it only fits the data in a very narrow region near maximum particle energy. The expected energies of ^{3}H from transitions to ^{5}Li (g.s.) and energies of ^{3}He from transitions to ^{5}He (g.s.) are marked with arrows in Fig. 5(b). The broad peak near the ^{5}Li and ^{5}He arrows may correspond to the sum of the ^{5}Li and ^{5}He transitions. However, considerably more data and analysis would be required before one could be sure of such details.

Figure 5(c) contains plots of the energy distributions for ^{4}He particles from the two breakup reactions. In this case there are no states of ^{4}He which could act as an intermediate state in a sequential decay, and so one expects no peaks in the ^{4}He spectrum arising from final-state interactions. Distortions of the phase-space distribution are expected from the decay of ^{7}Li, ^{5}Li, and ^{5}He intermediate states mentioned above, but recoil effects should distribute the ^{4}He decay product over a large part of the energy spectrum and make it difficult to recognize contributions from any particular source. Here, as with the mass-3 spectra, one expects our calculation of Coulomb effects to be appropriate only near the upper end of the spectrum.

The final matter we wish to address concerns our measurements of total cross sections. The total cross section for proton production in the $^6\mathrm{Li}(d,p^3\mathrm{H})^4\mathrm{He}$ reaction obtained from present measurements is plotted in Fig. 6. The results of Macklin and Banta[7] based on ^{3}H production from the same reaction are also plotted and are in excellent agreement with our measurements. Similarly, the total cross section for $^6\mathrm{Li}(d,n^3\mathrm{He})^4\mathrm{He}$ as obtained from the neutron measurements are given by the lower points of Fig. 6. We also have total cross sections for mass-3 (^{3}H and ^{3}He) particles and mass-4 (^{4}He) particles. It is easily seen that the total cross section for production of mass-3 particles, $\sigma_t(3)$, and for mass-4 particles, $\sigma_t(4)$, should be equal. Thus

$$\sigma_t(3)=\sigma_t(4)\,, \tag{3}$$

and

$$\sigma_t(p)+\sigma_t(n)=\sigma_t(3)\,, \tag{4}$$

in which $\sigma_t(p)$ is the total cross section for protons from $^6\mathrm{Li}(d,p^3\mathrm{H})^4\mathrm{He}$ and $\sigma_t(n)$ is the total cross section for neutrons from $^6\mathrm{Li}(d,n^3\mathrm{He})^4\mathrm{He}$. We have chosen to use these relationships to obtain another

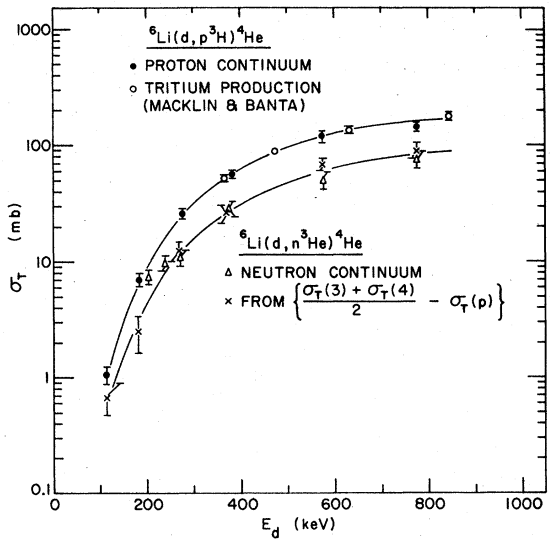

FIG. 6. Total cross sections for ^{6}Li$(d,p^3$H$)^4$He and ^{6}Li$(d,n^3$He$)^4$He as a function of deuteron bombarding energy. Also shown are the results of the activation measurements of Macklin and Banta.[8] A second determination of the neutron cross section is derived from the charged-particle data as described in the text, and plotted as points marked with an x.

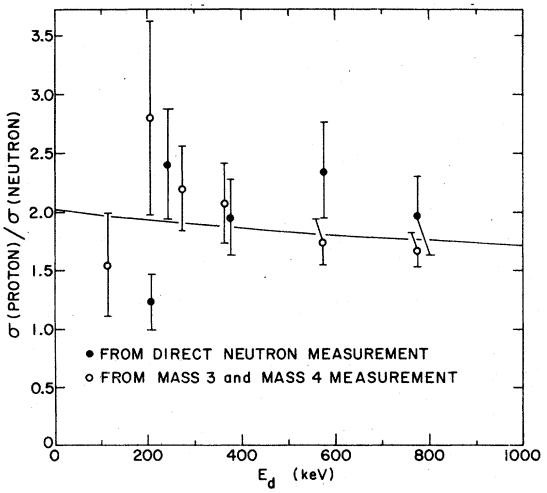

FIG. 7. The ratio of the total cross sections for ^{6}Li$(d,p^3$H$)^4$He and ^{6}Li$(d,p^3$He$)^4$He as a function of deuteron energy. The curve is calculated from the phase-space energy distributions as described in the text.

measure of the cross section for ^{6}Li$(d,n^3$He$)^4$He given by

$$\sigma_t'(n) = [\sigma_t(3) + \sigma_t(4)]/2 - \sigma_t(p) . \quad (5)$$

This is also plotted in Fig. 6 and gives an intercomparison between the neutron measurements and the charged-particle measurements. Again the agreement is within experimental error.

The ratio $\sigma_t(p)/\sigma_t(n)$ is plotted in Fig. 7 as a function of deuteron bombarding energy. Also shown in Fig. 7 is the ratio of the phase-space predictions for the total cross sections. This ratio can be easily computed in the center-of-mass system; it is unchanged by transformation to the laboratory system. Thus, at each deuteron energy, we obtain for the ratio

$$\sigma_t(p)/\sigma_t(n) = \int P_p(E)dE \Big/ \int P_n(E)dE$$

$$\propto [E_{\max}(p)/E_{\max}(n)]^2 . \quad (6)$$

All energies, cross sections, and energy distributions are taken in the center-of-mass system. The maximum kinematically allowed particle energy in the center-of-mass system is given by

$$E_{\max} = (Q + \tfrac{3}{4}E_d)(m_2 + m_3)/(m_1 + m_2 + m_3) ,$$

where Q is the reaction Q value, m_1 is the observed particle mass, m_2 and m_3 are masses of the unobserved particles, and E_d is the incident deuteron energy in the laboratory system. Equation (6) gives $\sigma_t(p)/\sigma_t(n) = 2.03$ for $E_d = 0$; the ratio slowly decreases as E_d increases. Although our data are consistent with this prediction, the errors in the experimental values are large, and other functions for this ratio could also fit the data.

The observation that the ratio of the measured total cross sections for protons and neutrons is apparently given by the ratio of their respective phase-space volumes does not necessarily imply that simultaneous, or direct, three-body breakup dominates these reactions. Indeed, we saw above that modifications to phase-space distributions due to Coulomb final-state interactions between the two unobserved particles lead to good representations of the shape of the individual spectra in the higher energy region. The results shown in Fig. 7 do suggest, however, that if any sequential-decay model is relevant to these three-body reactions, the important final-state interactions are expected to be similar for these charge-symmetric neutron and proton processes.

[1]A. J. Elwyn, R. E. Holland, F. J. Lynch, J. E. Monahan, and F. P. Mooring, in *Proceedings of the Conference on Nuclear Cross Sections and Technology*, NBS Special Publication No. 425 (National Bureau of Standards, Washington, D. C., 1975), Vol. I, p. 692.

[2]A. J. Elwyn, R. E. Holland, J. E. Monahan, C. N. Dav-

ids, L. Meyer-Schützmeister, F. J. Lynch and F. P. Mooring in *Scientific and Industrial Applications of Small Accelerators, IV Conference*, published as IEEE Report No. 76CH 1175-9NPS (IEEE, New York, 1976), p. 262.

[3]A. J. Elwyn, R. E. Holland, C. N. Davids, L. Meyer-Schützmeister, J. E. Monahan, F. P. Mooring and W. Ray, Jr., Phys. Rev. C 16, 1744 (1977).

[4]V. A. Crocker, S. Blow, and C. J. H. Watson, Culham Lab. Report No. CLM-P240, 1970 (unpublished); J. R. McNally, Jr., USAEC Report No. ORNL-TM-7647, 1974 (unpublished); J. R. McNally, Jr., USAEC Report No. ORNL-TM-4575, 1974 (unpublished); J. R. McNally, Jr., in *Proceedings of the Conference on Nuclear Cross Sections and Technology, Washington, D. C., 1975* (National Bureau of Standards, Washington, D. C., 1975), p. 683, and NBS Special Publication 425 (unpublished).

[5]See for example S. A. Colgate, J. Audouze and W. A. Fowler, Astrophys. J. 213, 849 (1977).

[6]S. H. Levine, R. S. Bender, and J. N. McGruer, Phys. Rev. 97, 1249 (1955); E. W. Hamburger and J. R. Cameron, *ibid.* 117, 781 (1960); J. C. Legg, W. D. Simpson, and S. T. Emerson, Nucl. Phys. A119, 209 (1968).

[7]M. Fricand and L. Marquez, J. Phys. (Paris) 27, 13 (1966); R. T. Frost and S. S. Hanna, Phys. Rev. 110, 939 (1958); N. A. Vlasov and A. A. Ogloblin, Zh. Eksp. Teor. Fiz. 37, 54 (1959) [Sov. Phys.—JETP 10, 39 (1960)]; S. Kato *et al.*, Nucl. Phys. A195, 534 (1972).

[8]R. L. Macklin and H. E. Banta, Phys. Rev. 97, 753 (1955).

[9]F. Ajzenberg-Selove and T. Lauritsen, Nucl. Phys. A227, 1 (1974).

[10]G. G. Ohlsen, Nucl. Instrum. Methods 37, 240 (1965).

[11]R. J. N. Phillips, Nucl. Phys. 53, 650 (1964).

[12]A. J. Elwyn, F. T. Kuchnir, J. E. Monahan, F. P. Mooring, J. F. Lemming, and W. G. Stoppenhagen Phys. Rev. C 6, 1730 (1972).